Out-of-plane (e,2e) angular distributions and energy spectra of helium $L = 0,1,2$ autoionizing levels

B. A. deHarak,[1] K. Bartschat,[2] and N. L. S. Martin[3]

[1]*Physics Department, Illinois Wesleyan University, P.O. Box 2900, Bloomington, Illinois 61702-2900, USA*

[2]*Department of Physics and Astronomy, Drake University, Des Moines, Iowa 50311, USA*

[3]*Department of Physics and Astronomy, University of Kentucky, Lexington, Kentucky 40506-0055, USA*

(Received 19 October 2010; published 8 December 2010)

Angular distribution and spectral (e,2e) measurements are reported for the helium autoionizing levels $(2s^2)^1S$, $(2p^2)^1D$, and $(2s2p)^1P$. A special out-of-plane geometry is used where the ejected electrons are emitted in a plane perpendicular to the scattered electron direction. The kinematics are chosen so that this plane contains the momentum-transfer direction. While the recoil peak almost vanishes in the angular distribution for direct ionization, it remains significant for the autoionizing levels and exhibits a characteristic shape for each orbital angular momentum $L = 0,1,2$. A second-order model in the projectile-target interaction correctly reproduces the observed magnitudes of the recoil peaks, but is a factor of 2 too large in the central out-of-plane region. Observed (e,2e) energy spectra for the three resonances over the full angular range are well reproduced by the second-order calculation. Calculations using a first-order model fail to reproduce both the magnitudes of the recoil peaks and the spectral line profiles.

DOI: 10.1103/PhysRevA.82.062705 PACS number(s): 34.80.Dp

I. INTRODUCTION

The (e,2e) technique investigates electron-impact ionization for the experimental case where the kinematics of both outgoing electrons are fully determined. An incident electron of energy E_0 (momentum $\boldsymbol{k}_0$) ionizes a neutral atom or molecule, producing a singly charged ion in the ground or excited state. For asymmetric kinematics, the two outgoing electrons have different energies, and, for the special case where one of the outgoing electrons is fast and the other is slow, they may be labeled "scattered" (sc) and "ejected" (ej), respectively. The two outgoing electrons of energy $E_{\rm sc}$ and $E_{\rm ej}$ (momenta $\boldsymbol{k}_{\rm sc}$ and $\boldsymbol{k}_{\rm ej}$) are detected in (delayed) coincidence at predetermined angles and energies, subject to the energy balance $E_0 = E_{\rm sc} + E_{\rm ej} + E_I$, where E_I is the threshold energy of the chosen final ion state. Experimental data are commonly presented as a set of (e,2e) angular distributions where the scattered-electron direction is fixed and the ejected-electron direction is varied. For the investigation of direct ionization, a typical set would span a range of kinematic conditions for the incident, scattered, and ejected electrons. For experiments on autoionizing levels, data may also be exhibited as (e,2e) energy spectra, and there have been a number of such studies on the $2\ell2\ell'$ autoionizing levels of helium [1–5]. The data are commonly presented in terms of the angular dependence of parameters fitted to generalized line profiles. These experiments, however, have been of the *coplanar* type, where the linear momentum of the ejected electron lies in the scattering plane formed by the momenta of the incident and scattered electrons, respectively (i.e., all three electron trajectories lie in the same plane). An *out-of-plane* (e,2e) experiment is one where the ejected electron is observed in directions that do not lie in the scattering plane. We recently reported out-of-plane (e,2e) angular distribution studies on He autoionizing levels [6]. Here, we present a more extensive report that includes measurements and calculations of out-of-plane (e,2e) energy spectra at selected ejected-electron angles.

Our out-of-plane experiments were motivated by the findings of two out-of-plane charged-particle impact ionization experiments on helium at high projectile energy [7,8]. At high incident energies, the ejected-electron angular distribution is expected to be well described by the plane-wave Born approximation (PWBA). A representative calculation for the direct ionization process

$$\mathrm{He}(1s^2) + P_0^{\pm} \rightarrow \mathrm{He}^+(1s) + P_{\rm sc}^{\pm} + e_{\rm ej}, \qquad (1)$$

where $P^{\pm}$ is the incident ion or electron, is shown in Fig. 1. The figure is a three-dimensional polar plot where the intensity of ejected electrons in a particular direction is proportional to the position vector to the surface in that direction. In the figure, plane I is the scattering plane, and plane II is perpendicular to both the momentum transfer $\boldsymbol{K} \equiv \boldsymbol{k}_0 - \boldsymbol{k}_{\rm sc}$ and the scattering plane. There are two main features, the large binary lobe and the smaller recoil lobe, which are both rotationally symmetric around $\boldsymbol{K}$. The relative size of the binary and recoil lobes in the PWBA is determined by the magnitude of the momentum transfer; Fig. 1 corresponds to a value of $K \approx 0.7$ a.u. (atomic units). In general, as K increases, the magnitude of the recoil lobe decreases relative to the binary lobe, and in the limit of large momentum transfer the recoil lobe vanishes.

In an experiment on He ionization by fast C^{6+} ions [7], the angular distribution of electrons ejected into the scattering plane agreed well with theory, but the angular distribution of those in plane II disagreed with expectations by a factor of between 3 and 5; no calculations to date have been able to satisfactorily reproduce these data. Somewhat smaller discrepancies were found in an (e,2e) experiment on helium carried out with equivalent kinematics [8]. Out-of-plane experiments on Mg [9,10] found dramatic deviations from the rotational symmetry about $\boldsymbol{K}$.

The experiments on He direct ionization are examples of three-body dynamics because the $1s$ electron common to the initial state $\mathrm{He}(1s^2)$ and the residual ion $\mathrm{He}^+(1s)$ is essentially a spectator [11]. Helium ionization-excitation, on the other hand, where the ion is left in an excited state $\mathrm{He}^+(n\ell)$ (where $\ell \geqslant 2$), is a four-body process and hence presents a much greater challenge to theory; coplanar experiments

 ©2010 The American Physical Society

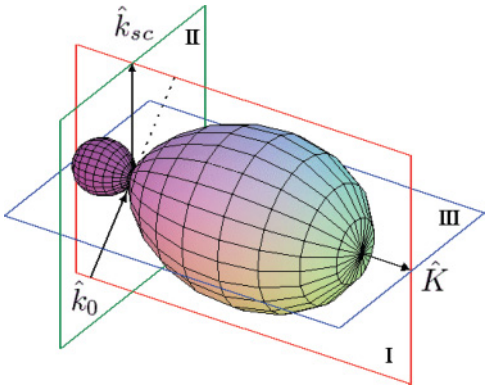

FIG. 1. (Color online) Representative PWBA calculation of an ejected-electron angular distribution for direct ionization. See text for details.

have recently investigated this process [11–13]. It was found that second-order models in the projectile-target interaction were essential to get good agreement when the two outgoing electrons had different energies. However, even these theories did not do so well for the case of symmetric energy sharing [14]. In fact, even the calculation of the total He ionization-excitation cross section remains a significant problem [15].

Here we present out-of-plane experiments on the three He singlet autoionizing levels $(2s^2)^1S$, $(2p^2)^1D$, and $(2s2p)^1P$. Table I lists the properties of these doubly excited $2\ell 2\ell'$ autoionizing levels with orbital angular momentum $L = 0,1,2$ [16–18]. The ionization process may be written as

$$\begin{array}{ccc} \mathrm{He}(1s^2) + e_0 & \longrightarrow & \mathrm{He}^+(1s) + e_{\mathrm{sc}} + e_{\mathrm{ej}}, \\ & \searrow\ \mathrm{He}\,(2\ell 2\ell')\ \nearrow & \end{array} \tag{2}$$

where there is interference between the amplitudes for direct ionization (upper path) and autoionization via an intermediate resonance (lower path) [19]. Thus, He autoionization by electron impact involves both direct ionization and the excitation of doubly excited resonances, and is an example of mixed three-body and four-body processes. Our experiments, therefore, test how well theory can describe three-body *and* four-body dynamics for out-of-plane kinematics.

Section II gives details of the theoretical calculations with which we compare our results. Section III describes the apparatus and the geometry of our out-of-plane measurements. Section IV presents the results, and Sec. V presents our conclusions.

TABLE I. Helium autoionizing levels and relevant parameters obtained from the literature [16–18]. E_L (where L is the orbital angular momentum of the level) is the energy above the ground state, E_{ej} is the corresponding ejected electron energy, and Γ_L is the level width.

	E_L (eV)	E_{ej} (eV)	Γ_L (meV)
$2s^2\ {}^1S_0$	57.84	33.25	120
$2p^2\ {}^1D_2$	59.91	35.32	57
$2s2p^1\ P_1$	60.15	35.56	38

II. THEORY

One of the first descriptions of electron-impact autoionization was given by Balashov *et al.* [20], who combined Fano's theory of autoionization [19] with a traditional plane-wave Born formalism. Since then, much work has been done using increasingly more sophisticated theories. For comparison with our angular distribution data, we have carried out both simple Balashov *et al.*–type PWBA calculations, and state-of-the-art first-order and second-order hybrid distorted-wave + convergent R-matrix with pseudostates (close-coupling) calculations (DWB1-RMPS and DWB2-RMPS, respectively). The distorted-wave theories were also used to calculate $(e,2e)$ ejected-electron energy spectra.

While the PWBA model is not expected to be quantitatively correct, it is useful in that the formalism developed by Balashov *et al.* [20] makes definite qualitative predictions about the effect of autoionization on the $(e,2e)$ ejected-electron angular distributions. Specifically, the triply differential cross section (TDCS) in the neighborhood of an isolated autoionizing resonance of angular momentum L is given (in a.u.) by

$$\frac{d^3\sigma}{d\hat{\boldsymbol{k}}_{\mathrm{ej}}\, d\hat{\boldsymbol{k}}_{\mathrm{sc}}\, dE_0} = \frac{4}{K^4}\frac{k_{\mathrm{sc}}}{k_0}|T(\boldsymbol{k}_{\mathrm{ej}},\boldsymbol{K})|^2, \tag{3}$$

where the amplitude is

$$T(\boldsymbol{k}_{\mathrm{ej}},\boldsymbol{K}) = t(\boldsymbol{k}_{\mathrm{ej}},\boldsymbol{K}) + t^{(L)}(\boldsymbol{k}_{\mathrm{ej}},\boldsymbol{K})\frac{q_L - i}{\varepsilon_L + i}. \tag{4}$$

Here q_L is the Fano resonance profile index [19] and ε_L is the energy away from the resonance position in units of the resonance half-width $\Gamma_L/2$. The direct ionization amplitude is $t(\boldsymbol{k}_{\mathrm{ej}},\boldsymbol{K})$, while $t^{(L)}(\boldsymbol{k}_{\mathrm{ej}},\boldsymbol{K})$ is the part of the direct ionization amplitude associated with the resonance. The latter is given by

$$t^{(L)}(\boldsymbol{k}_{\mathrm{ej}},\boldsymbol{K}) = c_L P_L(\cos\theta_0), \tag{5}$$

with

$$c_L = \frac{\int t(\boldsymbol{k}_{\mathrm{ej}},\boldsymbol{K}) P_L(\cos\theta_0) d\hat{\boldsymbol{k}}_{\mathrm{ej}}}{\int P_L(\cos\theta_0)^2 d\hat{\boldsymbol{k}}_{\mathrm{ej}}}, \tag{6}$$

where P_L is a Legendre polynomial and θ_0 is the angle between the ejected-electron direction and the momentum-transfer vector: $\cos\theta_0 = \hat{\boldsymbol{k}}_{\mathrm{ej}} \cdot \hat{\boldsymbol{K}}$. Details of our method for calculating $t(\boldsymbol{k}_{\mathrm{ej}},\boldsymbol{K})$, when plane waves are used to describe the incident, scattered, and ejected electrons (PPP), are given in Ref. [21]. In our model, q_L was left as an adjustable parameter to be fitted to the experimental data. We also carried out a slightly more sophisticated calculation that used plane waves to describe the incident and scattered electrons, but a distorted wave for the outgoing ejected electron (PPD). The results were almost identical to the PPP calculation except that a much lower value of q_0 was needed to agree with experiment; this has been discussed elsewhere [22].

For *direct* ionization, the PWBA (and all other theories) predicts that as K increases, the intensity of the recoil peak decreases relative to that of the binary peak, and for the kinematics of our present experiments, where $K \approx 2$ a.u., it essentially vanishes. However, when autoionization is present, the second term in Eq. (4) does not vanish. The recoil peak, therefore, remains significant and exhibits a specific shape determined by the angular momentum L of the autoionizing

state via the P_L dependency of $t^{(L)}(\boldsymbol{k}_{\rm ej}, \boldsymbol{K})$. Thus, each of the three He autoionizing levels ($L = 0,1,2$) is expected to leave a characteristic signature in the shape of a recoil peak with behavior given by $(P_L)^2$.

Details of the DWB1-RMPS and DWB2-RMPS methods are given elsewhere [23–26]. The essential point is that the (fast) projectile-target interaction is treated perturbatively to first (DWB1) or second (DWB2) order, while the initial bound state and the e−He$^+$ half-collision of a slow ejected electron and the residual ion are treated via a convergent close-coupling expansion. An analysis of our calculations, in terms of effective Fano q parameters of the resonant partial waves, is given elsewhere [22]. It is found that the q_L parameters for the first-order calculations are real, whereas those of the second-order calculations are complex, but with real parts similar to the first-order values. When the resonant $\ell = L$ partial waves with complex q_L are combined with the nonresonant $\ell \neq L$ partial waves, they result in angular distributions—and, most importantly, spectral line profiles—that are very different from those of the first-order calculations.

III. EXPERIMENTAL

The experimental apparatus is described in detail elsewhere [4,27]. It is a formerly coplanar apparatus that has been modified to perform a special type of out-of-plane measurement. It consists of an unmonochromated electron gun, a gaseous target beam (emitted from a 0.5 mm internal diameter molybdenum tube that is attached to, and hence moves with, the electron gun mount), two ejected-electron spectrometers, and a scattered-electron spectrometer. The two ejected-electron spectrometers are mounted 180° apart on a turntable, and the scattered-electron spectrometer is mounted on a second, concentric and coplanar, turntable.

All three spectrometers are similar and consist of electron optics that transport and focus the electrons from the interaction region into the entrance slits (ejected-electron spectrometers) or aperture (scattered-electron spectrometer) of hemispherical-sector electrostatic energy analyzers. Each ejected-electron analyzer is terminated by a microchannel plate (MCP) assembly followed by a position sensitive detector (PSD) consisting of a resistive anode. The outputs of the two PSDs are fed to the same position decoding electronics (PDE). The scattered detector is terminated by a high-count channeltron. The fast ejected-electron MCP signals, and the fast scattered-electron signal from the channeltron, are fed to three independent sets of NIM units that provide fast output signals for (delayed) coincidence timing, and also enable the PDE output (via a simple logic gate) to be assigned to the appropriate ejected-electron spectrometer.

The geometry of the apparatus, as used in the present experiments, is shown in Fig. 2. With reference to the Cartesian coordinates shown in the diagram, the scattered- and ejected-electron detectors are fixed so as to accept electrons in the directions $\hat{\boldsymbol{k}}_{\rm sc} = \hat{\boldsymbol{z}}$ and $\hat{\boldsymbol{k}}_{\rm ej} = \pm\hat{\boldsymbol{x}}$, respectively. The gun moves on the surface of a cone with axis $\hat{z}$, and of half-angle equal to the scattering angle $\theta_{\rm sc}$. In terms of a spherical coordinate system, as the gun rotates, its position is described by the polar angle $\theta = \theta_{\rm sc} = {\rm const}$ and variable azimuthal angle ϕ. This geometry is equivalent to rotating the

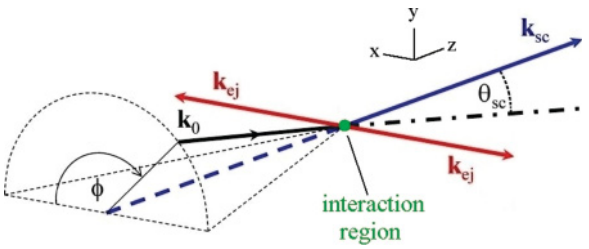

FIG. 2. (Color online) Geometry of the apparatus. The incident ($\boldsymbol{k}_0$) and detected ejected- ($\boldsymbol{k}_{\rm ej}$) and scattered- ($\boldsymbol{k}_{\rm sc}$) electron directions are indicated.

ejected-electron detectors around z while keeping the gun and scattered-electron detector fixed. Thus, as the gun position is varied from $\phi = 0° \rightarrow 180°$, the ejected detector on the left effectively varies from $\phi_{\rm ej} = 0° \rightarrow -180°$, and the ejected detector on the right effectively varies from $\phi_{\rm ej} = 180° \rightarrow 0°$, with a combined range equal to the full $\phi_{\rm ej} = 0° \rightarrow 360°$. In fact, reflection symmetry in the scattering plane means that the angular distributions obtained by the two detectors should be mirror images of one another. Thus, having two ejected-electron detectors in our configuration doubles the effective count rate, and also enables a comparison of the two detectors and the determination of possible instrumental effects. Indeed, the measured angular distributions had to be corrected for the ϕ dependence of the instrument functions of the ejected- and scattered-electron detectors; the correction procedure is described in detail elsewhere [27].

We have carried out (e,2e) out-of-plane experiments for the special kinematical case where the momentum-transfer vector is perpendicular to the scattered-electron direction. For an incident electron of energy E_0, the condition for this is $\theta_{\rm sc} = \arcsin(\sqrt{\Delta E/E_0})$, where ΔE is the energy loss (i.e., the energy of the $2\ell 2\ell'$ autoionizing levels above the ground state ≈60 eV). The corresponding momentum transfer is $K = \sqrt{2\Delta E}$, which is independent of the initial energy and has the value $K = 2.1$ a.u. in the autoionizing region.

The experiments reported here were carried out with an incident electron energy $E_0 = 488$ eV, for which the desired scattering angle is $\theta_{\rm sc} = 20.5°$. With these kinematics, the measured (e,2e) out-of-plane angular distribution of ejected electrons corresponds to plane III of Fig. 1. This plane contains the momentum-transfer vector $\boldsymbol{K}$; it is perpendicular to $\boldsymbol{k}_{\rm sc}$ and hence also to the scattering plane. (Note that all ejected-electron directions $\hat{\boldsymbol{k}}_{\rm ej}$ in plane III are perpendicular to $\hat{\boldsymbol{k}}_{\rm sc}$.)

We report two types of experiments: (e,2e) ejected-electron angular distribution measurements, and (e,2e) spectral measurements at various ejected-electron directions. For the angular distribution measurements, the apparatus was tuned to accept electrons in a uniform energy window of 0.4 eV [4], and the theoretical predictions were energy integrated over the same window. The (e,2e) spectra were taken by scanning the pass energy of the spectrometers over each resonance while using the full resolution of the PSDs. For the present experiments, the energy resolution was degraded in order to increase the coincidence count rates. The calculated spectra were folded with the experimental resolution, which was found by fitting the noncoincident ejected-electron spectra to generalized line shapes, as was done in earlier work [4]. The spectral resolution

varied from 100 to 170 meV for the different angles; this variation is probably due to drifts in the energy scales during the long run times necessary—each angular distribution, and each spectrum, took several days to accumulate.

IV. RESULTS AND DISCUSSION

Our experimental results and theoretical predictions are shown in Figs. 3 and 4. The $(e,2e)$ angular distributions are shown in Fig. 3 for direct ionization and the three autoionizing levels. The binary peak position (i.e., momentum-transfer direction) corresponds to $\phi = 0$, and therefore ϕ is numerically equal to θ_0, the angle, defined above, between the momentum-transfer vector and the ejected-electron direction. The recoil peak position is therefore at $\phi = 180^\circ$, but all other angles lie outside the scattering plane (see plane III of Fig. 1). All experimental data and calculations were normalized to unity at the binary peak of each individual angular distribution.

Figure 3(a) is the angular distribution for direct ionization. The PWBA underestimates the width of the binary peak, whereas both the DWB1-RMPS and DWB2-RMPS calculations are in good agreement with experiment over the entire angular range, within the statistics of the present experiment. The data show conclusively that the recoil peak is extremely small, and we therefore expect autoionization to have a profound effect on this part of the angular distribution. That this is indeed the case is seen in Figs. 3(b)–3(d), which show the angular distributions of the ^1S, ^1D, and ^1P autoionizing levels. For the PWBA calculations, values of q_L were chosen to give the correct recoil peak intensities. The resultant curves agree quite well with the experimental data, with fitted values $q_0 = -15$, $q_1 = -6.3$, and $q_2 = -4.8$. These are larger by factors of between 3 and 8 than first-order calculated values found in the literature [28]—this possibly indicates the need for a second-order calculation of q_L that treats the four-body projectile-target interaction more completely. The exceptionally large magnitude of q_0 is an artifact of using a plane wave with Gram-Schmidt orthogonalization for the ejected-electron wave function. Repeating the PWBA calculations with distorted waves for the ejected-electron wave functions yields almost identical angular distributions with fitted values of q_1 and q_2 within 10% of the above values, but a value $q_0 = -3$, which is a difference of a factor of 5 [22].

As predicted, a comparison of the PWBA predictions with the data shows that each autoionizing level has a signature described by the behavior of the appropriate $(P_L)^2$. In Fig. 3(b) the data for ^1S are clearly nonzero over the entire angular range, as expected from $(P_0)^2 = \text{const}$. Both the ^1D and ^1P angular distributions in Figs. 3(c) and 3(d) show pronounced recoil peaks and minima close to 90°, and the data in the range $\phi = 60^\circ \rightarrow 135^\circ$ are consistent with the behavior of $(P_2)^2$ and $(P_1)^2$, respectively. The first-order DWB1-RMPS model does a good job for $\phi = 45^\circ \rightarrow 135^\circ$, but it severely underestimates the magnitudes of the recoil peaks. On the other hand, the second-order DWB2-RMPS calculations are in excellent agreement with the data in the recoil peak for all three autoionizing levels, but are about a factor of 2 too large in the out-of-plane region $\phi = 45^\circ \rightarrow 90^\circ$ for the ^1D and ^1P levels. Note that when autoionization is *absent*, these two theories also disagree by a factor of 2 in this region [see Fig. 3(a)]. This may be responsible, via the interference term, for the similar disagreement in Figs. 3(c) and 3(d).

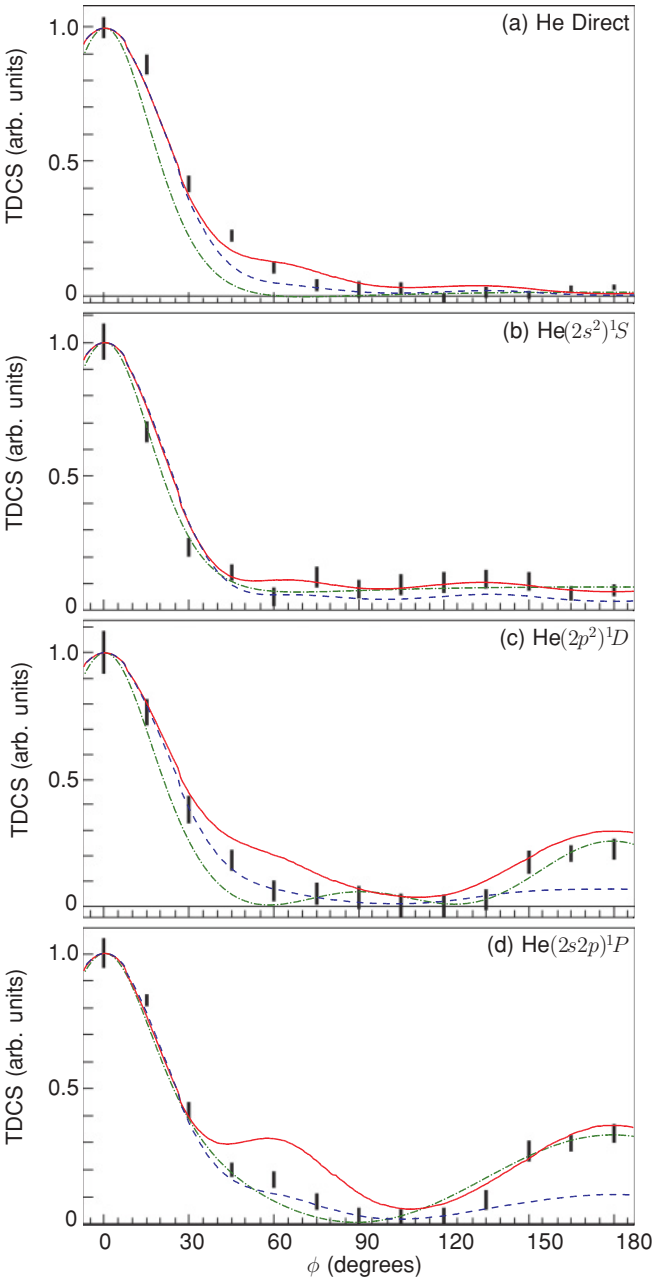

FIG. 3. (Color online) Helium out-of-plane $(e,2e)$ ejected-electron angular distributions for 488 eV electrons scattered through 20.5°. The vertical bars represent the experimental results and include both statistical and systematic errors. (a) Direct ionization with 34.1 eV ejected electrons. (b)–(d) Direct ionization plus autoionization via $(2s^2)^1S$, $(2p^2)^1D$, and $(2s2p)^1P$. The solid (red) and dashed (blue) lines are DWB2-RMPS and DWB1-RMPS calculations, respectively, while the dot-dashed (green) lines are fitted PWBA calculations described in the text. Theory and experiment are normalized to unity at $\phi = 0$.

Figure 4 shows experimental and theoretical $(e,2e)$ spectra taken at 30° intervals between the binary and recoil peaks (i.e., at angles corresponding to every other data point of Fig. 3). We have attempted to obtain roughly equal statistical experimental uncertainties at all angles. This required exceptionally long run

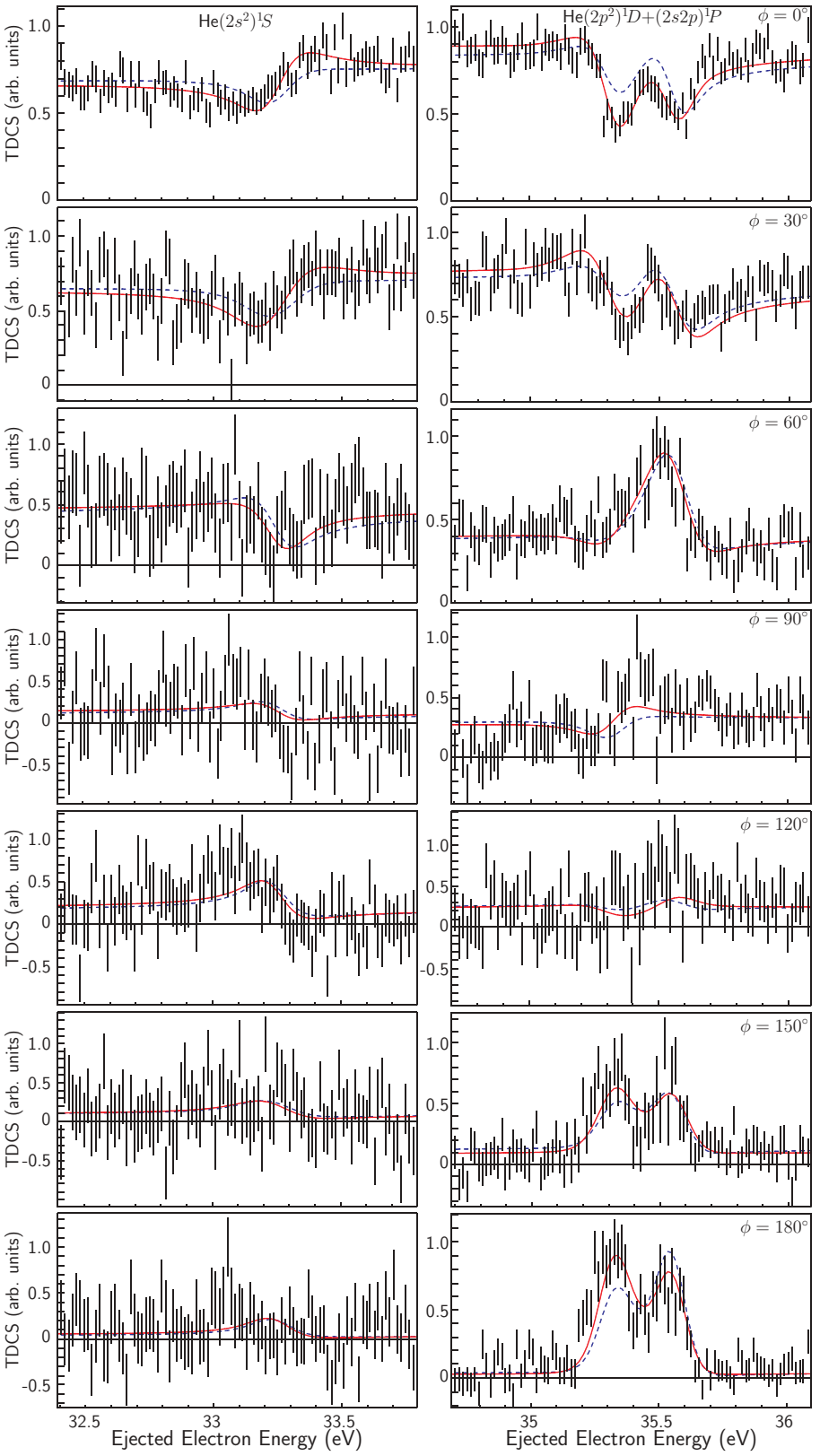

FIG. 4. (Color online) Helium out-of-plane (e,2e) autoionizing spectra for 488 eV electrons scattered through 20.5° and selected values of ϕ. The vertical bars represent the experimental results and their statistical errors. The solid (red) and dashed (blue) lines are DWB2-RMPS and DWB1-RMPS calculations, respectively. Each theory and experiment is scaled to each other by a least-chi-squares fit.

times at, for example, $\phi = 90°$ compared with those at $\phi = 0$. Even so, the spectra taken at the former angle are relatively poor. Each panel in the figure has been arbitrarily normalized to the maximum data point. Since this part of the experiment was designed to compare spectral line shapes, each theory has then been scaled separately by a simple single parameter least-chi-squares fit to the data, rather than by using the relative magnitudes of Fig. 3.

The spectra for $\phi = 0$ show that, even in the binary peak, the second-order calculation is in much better agreement with

experiment than the first-order calculation. This is perhaps surprising, given that the nonresonant partial waves, for which the first-order and second-order calculations are similar, dominate in the binary peak. However, it is the cross terms between these and the resonant terms that give rise to the spectral line shapes, and hence a second-order calculation is still necessary to obtain agreement with experiment, even at $\phi = 0$.

In fact, the second-order calculations are in better agreement than the first-order calculations with the data for all angles where the statistics enable a definite conclusion to be reached. In particular, the relative intensities of the ^1D and ^1P line shapes are well predicted by the second-order calculation. This is especially noticeable in the recoil peak ($\phi = 180^\circ$) for which the first-order calculation has the intensity ratio inverted. There is some evidence that the ^1S line shape is not well reproduced by either calculation for angles greater than 60°, but the statistics preclude any definite conclusion from being reached.

V. SUMMARY AND CONCLUSIONS

We have measured out-of-plane angular distributions for He direct ionization and $L = 0,1,2$ autoionizing levels, and have obtained spectra of the levels for selected angles. For direct ionization, a three-body process, both first-order and second-order distorted-wave calculations give an adequate description, as was true for out-of-plane experiments on Mg [9,10]. We find that the presence of autoionization has a dramatic effect on the angular distribution, as predicted by Balashov *et al.* [20], with each autoionizing resonance presenting its own, L-dependent, "signature." In a comparison of experiment and theory, two regions are of particular interest: a central, fully out-of-plane, region $\phi = 45^\circ \rightarrow 135^\circ$, and the recoil peak $\phi = 135^\circ \rightarrow 180^\circ$, which intersects the coplanar region along $-\hat{\boldsymbol{K}}$. For an incident energy of 488 eV and a momentum transfer of 2.1 a.u., we find that a second-order model in the projectile-target interaction is necessary to correctly reproduce the magnitude of the recoil peak when autoionization is present; the corresponding first-order model underestimates the magnitude by a factor of 3. A second-order model is also necessary to reproduce the spectral line profiles and the relative intensity of ^1D and ^1P. This need for a higher-order description is consistent with the findings of the excitation-ionization experiments (i.e., four-body processes) mentioned above [11–13]. However, neither the DWB2-RMPS nor the DWB1-RMPS model is able to reproduce the data over the full $0^\circ \rightarrow 180^\circ$ out-of-plane range; DWB2-RMPS is good in the recoil peak but not satisfactory in the central region, while the opposite is true for DWB1-RMPS. For our kinematics, therefore, we conclude that current sophisticated theories are still not entirely adequate for out-of-plane experiments on He autoionization. Experiments and calculations are planned for lower incident energies where the out-of-plane region is expected to be more important.

ACKNOWLEDGMENTS

This work was supported by the United States National Science Foundation under Grants No. PHY-0855040 (N.L.S.M.) and No. PHY-0757755 (K.B.).

[1] A. Crowe, D. G. McDonald, S. E. Martin, and V. V. Balashov, Can. J. Phys. **74**, 736 (1996).
[2] M. J. Brunger, O. Samardzic, A. S. Kheifets, and E. Weigold, J. Phys. B **30**, 3267 (1997).
[3] O. Samardzic, L. Campbell, M. J. Brunger, A. S. Kheifets, and E. Weigold, J. Phys. B **30**, 4383 (1997).
[4] B. A. deHarak, J. G. Childers, and N. L. S. Martin, J. Electron Spectrosc. Relat. Phenom. **141**, 75 (2004).
[5] O. Sise, M. Dogan, I. Okur, and A. Crowe, J. Phys. B **43**, 185201 (2010).
[6] B. A. deHarak, K. Bartschat, and N. L. S. Martin, Phys. Rev. Lett. **100**, 063201 (2008).
[7] M. Schulz, R. Moshammer, D. Fischer, H. Kollmus, D. H. Madison, S. Jones, and J. Ullrich, Nature (London) **422**, 48 (2003).
[8] M. Dürr, C. Dimopoulou, B. Najjari, A. Dorn, and J. Ullrich, Phys. Rev. Lett. **96**, 243202 (2006).
[9] R. W. van Boeyen, N. Watanabe, J. W. Cooper, J. P. Doering, J. H. Moore, and M. A. Coplan, Phys. Rev. A **73**, 032703 (2006).
[10] M. Foster, J. L. Peacher, M. Schulz, D. H. Madison, Z. Chen, and H. R. J. Walters, Phys. Rev. Lett. **97**, 093202 (2006).
[11] S. Bellm, J. Lower, K. Bartschat, X. Guan, D. Weflen, M. Foster, A. L. Harris, and D. H. Madison, Phys. Rev. A **75**, 042704 (2007).
[12] G. Sakhelashvili, A. Dorn, C. Höhr, J. Ullrich, A. S. Kheifets, J. Lower, and K. Bartschat, Phys. Rev. Lett. **95**, 033201 (2005).
[13] S. Bellm, J. Lower, and K. Bartschat, Phys. Rev. Lett. **96**, 223201 (2006).
[14] K. Bartschat, I. Bray, D. V. Fursa, and A. T. Stelbovics, Phys. Rev. A **76**, 024703 (2007).
[15] O. K. Vorov and K. Bartschat, J. Phys. B **38**, 1189 (2005).
[16] K. Schulz, G. Kaindl, M. Domke, J. D. Bozek, P. A. Heimann, A. S. Schlachter, and J. M. Rost, Phys. Rev. Lett. **77**, 3086 (1996).
[17] J. P. van den Brink, G. Nienhuis, J. van Eck, and H. G. M. Heideman, J. Phys. B **22**, 3501 (1989).
[18] B. A. deHarak, J. G. Childers, and N. L. S. Martin, Phys. Rev. A **74**, 032714 (2006).
[19] U. Fano, Phys. Rev. **124**, 1866 (1961).
[20] V. V. Balashov, S. S. Lipovetskii, and V. S. Senashenko, Sov. Phys. JETP **36**, 858 (1973).
[21] B. A. deHarak, Z. Chen, D. H. Madison, and N. L. S. Martin, J. Phys. B **38**, L145 (2005).
[22] N. L. S. Martin, B. A. deHarak, and K. Bartschat, J. Phys. B **42**, 225201 (2009).
[23] K. Bartschat and P. G. Burke, J. Phys. B **20**, 3191 (1987).
[24] R. H. G. Reid, K. Bartschat, and A. Raeker, J. Phys. B **31**, 563 (1998); **33**, 5261 (2000).
[25] Y. Fang and K. Bartschat, J. Phys. B **34**, L19 (2001).
[26] K. Bartschat and A. N. Grum-Grzhimailo, J. Phys. B **35**, 5035 (2002).
[27] B. A. deHarak and N. L. S. Martin, Meas. Sci. Technol. **19**, 015604 (2008).
[28] A. S. Kheifets, J. Phys. B **26**, 2053 (1993).